

Crystal Structure Analysis and in Silico pK_a Calculations Suggest Strong pK_a Shifts of Ligands as Driving Force for High-Affinity Binding to TGT

Tina Ritschel,^[a] Simone Hoertner,^[b] Andreas Heine,^[a] François Diederich,^[b] and Gerhard Klebe^{*[a]}

A novel ligand series is presented to inhibit tRNA-guanine transglycosylase (TGT), a protein with a significant role in the pathogenicity mechanism of *Shigella flexneri*, the causative agent of Shigellosis. The enzyme exchanges guanine in the wobble position of tRNA^{Asn,Asp,His,Tyr} against a modified base. To prevent the base-exchange reaction, several series of inhibitors have already been designed, synthesized, and tested. One aim of previous studies was to address a hydrophobic pocket with different side chains attached to the parent skeletons. Disappointingly, no significant increase in binding affinity could be observed that could be explained by the disruption of a conserved water cluster. The ligand series examined in this study are based on the known scaffold lin-benzoguanine. Different side chains were introduced leading to 2-amino-lin-benzoguanines, which address a different pocket of the protein and avoid disruption of the water cluster. With the introduction of an amino group in the 2-position, a dramatic increase in binding affinity can be experienced. To explain this significant gain in binding affinity, Poisson-Boltzmann calcu-

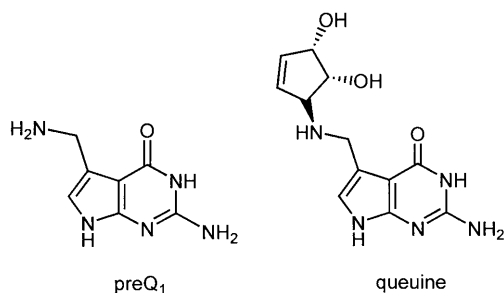
lations were performed to explore pK_a changes of ligand functional groups upon protein binding, they can differ significantly on going from aqueous solution to protein environment. For all complexes, a permanent protonation of the newly designed ligands is suggested, leading to a charge-assisted hydrogen bond in the protein-ligand complex. This increased strength in hydrogen bonding takes beneficial effect on binding affinity of the ligands, resulting in low-nanomolar binders. Crystal structures and docking emphasize the importance of the newly created charge-assisted hydrogen bond. A detailed analysis of the crystal structures in complex with substituted 2-amino-lin-benzoguanines indicate pronounced disorder of the attached side chains addressing the ribose 33 binding pocket. Docking suggests multiple orientations of these side chains. Obviously, an entropic advantage of the residual mobility experienced by these ligands in the bound state is beneficial and reveals an overall improved protein binding.

Introduction

During post-transcriptional modification, the prokaryotic enzyme tRNA-guanine transglycosylase (TGT, EC 2.4.2.29) catalyzes the exchange of guanine by the modified base preQ₁ (7-methylamino-7-deazaguanine) at the wobble position 34 of the anticodon loop of tRNA^{Asn,Asp,His,Tyr} (Scheme 1).^[1] Subsequently, the incorporated preQ₁ is further modified to queuine (7-(((4,5-*cis*-dihydroxy-2-cyclopenten-1-yl)amino)methyl)-7-deazaguanine), involving further enzymes in the biochemical pathway. The resulting tRNAs play a significant role in developing

pathogenicity of *Shigella flexneri*, the causative agent of Shigellosis. Shigellosis is responsible for about 165 million infections and causes more than one million fatalities each year. A high rate of incidences is observed among children at the age of one to four, predominantly in developing countries with poor hygienic conditions and unsafe water supplies.^[2,3] Increasing problems with respect to an administered drug therapy arise due to plasmid-encoded resistances against most common antibiotics and due to the lack of effective vaccines. In previous studies, the TGT gene of *S. flexneri* was knocked out leading to a significantly decreased infection rate.^[4] As an alternative prospective, we embarked upon the development of *Shigella*-specific antibiotics that prevent the evolution of pathogenicity.

The bacterium carries a virulence plasmid as source of its pathogenicity that encodes for a variety of virulence factor



Scheme 1. Structure of preQ₁, which replaces guanine 34 in the wobble position of the modified tRNA^{Asn,Asp,His,Tyr} during the base-exchange reaction of TGT. The precursor preQ₁ is further modified to queuine.

[a] T. Ritschel, Dr. A. Heine, Prof. Dr. G. Klebe
 Institut für Pharmazeutische Chemie, Philipps-Universität Marburg
 Marbacher Weg 6, 35032 Marburg (Germany)
 Fax: (+ 49) 6421-2828994
 E-mail: klebe@mail.uni-marburg.de

[b] Dr. S. Hoertner, Prof. Dr. F. Diederich
 Laboratorium für Organische Chemie, ETH-Zürich
 Hönggerberg, HCI, 8093 Zürich (Switzerland)

genes. Essential for the regulation of the pathogenicity-developing process of *Shigella* is the expression of the virulence factor VirF, which activates directly the transcription of further virulence genes such as *icsA* and *virB*.^[5] The modified tRNAs are required for an efficient translation of virF-mRNA at the ribosome. Reducing the amount of modified tRNA by preventing the base-exchange reaction provides a novel strategy for an antibiotic therapy. The bacterium is blocked from access of the endothelial cells, which is a prerequisite to create pathogenicity. This mode of action prevents eradication or any other influence in the function of the bacteria.

By means of structure-based drug design, we started the discovery of TGT-specific inhibitors. As the protein of the pathogenic organism *S. flexneri* is difficult to crystallize, we performed all the studies described in this contribution by using the better-crystallizing enzyme from *Zymomonas mobilis*. It exhibits an active site of almost identical composition. Only Phe106 is exchanged by Tyr.^[6]

TGT adopts a folding comparable to the highly populated triose-phosphate isomerase (TIM)-type ($\beta\alpha$)₈-barrel fold. Two insertions are responsible for the recognition of the substrate.^[7] The active site of TGT is located at the C-terminal end of the TIM-barrel scaffold and recognizes specially the trinucleotide sequence U₃₃G₃₄U₃₅.^[8,9,10] Uracil 33 and 35 are bound in a rather flat, solvent-exposed binding pocket. In contrast, the guanine binding pocket is very deep. Several hydrogen bonds are formed to Leu231, Ala230, Gln203, Asp156, and Asp102 along with a pronounced parallel π -stacking to Tyr106 flanking the binding site (Figure 1 A).

The pathway of the base-exchange reaction follows a ping-pong mechanism. Initiated by a nucleophilic attack of Asp280 towards C1' of ribose 34, a covalent intermediate is produced without breaking the phosphodiester backbone of tRNA.^[11,12] Simultaneously, guanine 34 is cleaved from the tRNA backbone leaving the binding pocket, subsequently. The vacant binding site now provides access for the modified base preQ₁ (Scheme 1). This nucleobase exhibits an extracyclic amino function, which replaces a water molecule that was previously mediating an interaction between protein and guanine. In the course of the mechanism, a flip of the peptide backbone is necessary to exchange the binding-site-exposed hydrogen-bonding facility from a donor to acceptor group to correctly recognize the new substrate. The peptide bond between Leu231 and Ala232 rearranges and performs an interaction via its carbonyl group to the extracyclic amino function of preQ₁ (Figure 1 A). A covalent bond between preQ₁ and tRNA is formed and the modified tRNA is released from the catalytic site. The described reaction path requires Asp102 and a close-by water molecule as general base.

Taking into account the physico-chemical properties of the guanine binding site, several lead structures have been designed and synthesized. Pyridazinones, pteridines, and quinoxalinones emerged as promising scaffolds (Table 1). In addition, a "stretched" guanine with an inserted central six-membered ring leading to *lin*-benzoguanine (**3**) was suggested (Table 2).^[13–15] All parent scaffolds bind in the micromolar range. To improve their binding affinity, a hydrophobic subpocket composed of Val282, Leu68, and Val45 was addressed. Filling

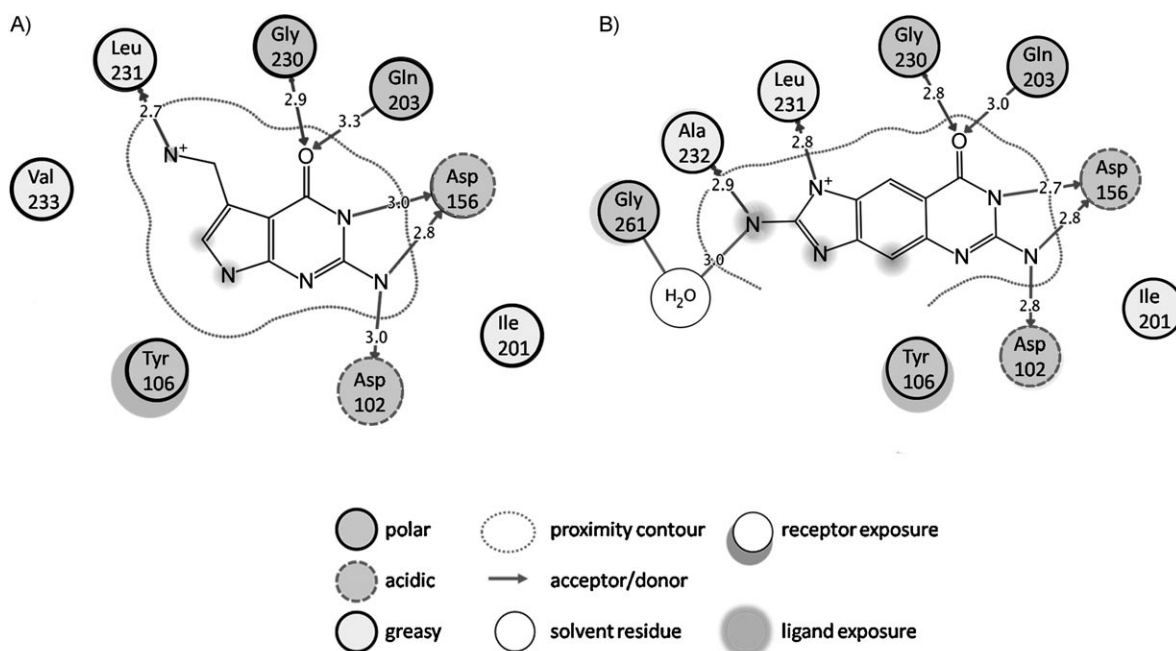
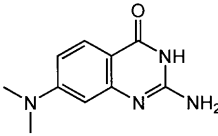
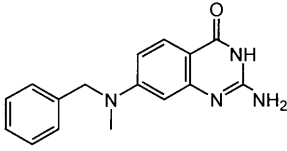


Figure 1. Schematic interaction pattern derived by MOE.^[36,37] For clarity, the hydrogen atoms are not shown. A) preQ₁ (PDB ID: 1P0E) in the guanine binding pocket. The protonated exocyclic amino function of the modified base forms a hydrogen bond to Leu231 (2.7 Å). A hydrogen bond network between the pyrimidine ring and Gly230, Gln203, Asp156, and Asp102 (bond length in Å) is responsible for the recognition of the modified base. B) **5** in the guanine binding pocket with two hydrogen bonds between the newly introduced guanidinium group and Leu231 (2.8 Å) and Ala232 (2.9 Å) of TGT. The positive charge, which is delocalized through the conjugated system of the guanidinium moiety is presented on N1 forming a charge-assisted hydrogen bond to Leu231. Furthermore, the ligand is fixed in the binding pocket by the above-described hydrogen bonds to Gly230, Gln203, Asp156, and Asp102 (bond length in Å). Mediated by a water molecule, an additional interaction to Gly261 is observed.

Table 1. Inhibitors based on a quinazolinone scaffold and their measured binding affinity.

Compound	Structure	Enzyme K_i
1		$(31 \pm 10) \mu\text{M}$
2		$(7.6 \pm 3.7) \mu\text{M}$

of unoccupied hydrophobic pockets with lipophilic side chains attached to the lead skeleton is an often-used strategy in structure-based drug design. Disappointingly, only an insignificant improvement in binding affinity towards TGT could be measured for inhibitors with a lipophilic side chain attached to the above-mentioned parent skeletons. A comprehensive study of crystal structures elucidated that the lipophilic vector disrupts a highly conserved water network between the catalytic aspartates (Figure 2B).^[14] This water network provides an essential contribution to the solvation of the two acidic residues.

Parallel to the synthesis of the inhibitors with the lipophilic vector, quinazolinones with a substitution in 7-position were prepared (Table 1). The introduction of a dimethylamino group produced **1** as two-digit micromolar inhibitor. Subsequent replacement of one methyl group by a benzyl moiety (**2**) resulted in a fourfold increase in binding affinity. Obviously, introduction of the sterically more demanding lipophilic side chain did not result in a loss of affinity in this case. The crystal structure of **2** in complex with TGT demonstrates that the water network is not perturbed by the benzyl moiety.^[16] Instead of addressing the small hydrophobic subpocket, the benzyl moiety binds most likely towards the region occupied by ribose 33 in the natural tRNA substrate as observed for the other ligands.

Stimulated by these promising results, we changed our design strategies now addressing the binding site of ribose 33 instead of the small hydrophobic pocket. This should avoid a disruption of the water cluster network. *lin*-Benzoguanine was again chosen as the parent scaffold; however, now focussing on substituents in the 2-position. The crystal structure of unsubstituted *lin*-benzoguanine in complex with TGT has been previously determined.^[14] Its binding mode is similar to that of preQ₁ (Figure 1A) and no interference with the water cluster network is observed. Additionally, substitution of *lin*-benzoguanine in 2-position provides the desired side chain orientation to address the ribose 33 subpocket. Several inhibitors with alkyl, alkylamino, and arylalkylamino substituents were synthesized and tested.^[15] The mixture of small and large side chains provided the possibility to experimentally investigate the influence of the side chain on the Gibbs free energy of binding.

Here, we present affinity data and crystallographic results of the newly designed inhibitors. In addition, we emphasize the introduction of a salt bridge between Leu231 and N1 of the inhibitor which finally bore nanomolar inhibitors.

Results and Discussion

Binding mechanism and affinity data

A series of 2-substituted *lin*-benzoguanines was synthesized and kinetically characterized (Table 2). Before the enzyme assay was performed, the binding mechanism was investigated by a trapping experiment.^[17] For the newly synthesized inhibitors (**4**–**10**), a purely competitive binding mechanism was found. The inhibitors can only bind to TGT when no tRNA is bound. A simultaneous binding of inhibitor and tRNA, as detected for **3**, can be excluded. Obviously, substitution with a single methyl group in 2-position makes the skeleton already large enough to avoid any contemporaneous binding of tRNA and inhibitor.

The affinity is determined by the exchange rate of guanine against [8-³H]-guanine in position 34 of tRNA^{Tyr}. The inhibitory constants are calculated based on the decrease of the initial velocity of the base-exchange reaction in presence of the inhibitor.

By introduction of a methyl group in 2-position (**4**) a 2.7-fold increase in binding affinity could be measured compared to the unsubstituted *lin*-benzoguanine (**3**). In an optimal situation, correct placement of a single methyl group can increase affinity up to tenfold, particularly when the surface of the added methyl group is entirely buried.^[18] According to the crystal structure of **3**, the guanine binding pocket provides additional space for the methyl group.

The addition of an amino group in 2-position creates a guanidinium-type moiety at our parent scaffold. From a synthesis point of view, it provides a convenient anchoring point to decorate the lead skeleton with a broad variety of side chains. Surprisingly, a dramatic increase in binding affinity towards TGT was recorded upon replacement of the methyl by an amino group. A 20-fold higher affinity was measured for **5** compared to **4**. Subsequent addition of a further methyl group enhances the affinity by 1.3-fold. With larger substituents at the nitrogen atom, the affinity gradually improves towards one-digit nanomolar range, as achieved by **9** and **10** (Table 1). Referring to the previously determined crystal structure of **3** in complex with TGT, the introduced guanidinium functionality offers the opportunity to form a hydrogen bond to the peptide backbone carbonyl group of Leu231.^[15] Considering the basic character of a guanidinium group, a protonation of this functional group in the ligand appears most likely. In consequence there would be a positive charge created on this portion of ligands **5**–**10**. It will be delocalized through the conjugated system of the ligand and should provoke, due to charge assistance, an increasing strength of the hydrogen bond between the ligand and the carbonyl group of Leu231. As a crude test of this hypothesis, the experimental pK_a values of ligand **3**–**9** were determined in aqueous solution.^[15] They actually point in the direction for increasing basicity. However, as the situation in a

Table 2. Structures of the inhibitors based on a *lin*-benzoguanine scaffold, and the corresponding inhibition constants determined by the enzyme assay, and pK_a values for the deprotonation of the imidazolium moiety in the parent scaffold.

Compound	Structure	Enzyme K_i	Experimental $pK_a^{[a]}$	Calculated $pK_a^{[a]}$	ΔpK_a shift ^[b]
3		$(4.1 \pm 1) \mu M$	5.2	7.2	2.0
4		$(1.5 \pm 0.4) \mu M$	5.4	7.5	2.1
5		$(77 \pm 12) nM$	6.3	8.3	2.0
6		$(58 \pm 36) nM$	6.2	8.6	2.4
7		$(35 \pm 9) nM$	5.8	7.4	1.6
8		$(55 \pm 11) nM$	5.9	7.0	1.1
9		$(6 \pm 6) nM$	5.3	6.5	1.3
10		$(10 \pm 3) nM$	–	–	–

[a] For **3–9**, experimental pK_a values for imidazolium deprotonation were measured in aqueous solution and, additionally, the pK_a values of the inhibitors in complex with TGT were calculated. [b] The shift of the pK_a values equals the difference between calculated and experimental ones.

water environment is not of relevance to the present case, and the protein environment can provoke pK_a shifts of several logarithmic units, Poisson–Boltzmann calculations within the binding pocket are performed based on our recently introduced peoe_pb (partial equalization of orbital electronegativities for Poisson–Boltzmann calculations) charges.^[19]

In silico pK_a calculation

The influences of specific charge distributions in protein binding sites are often ignored when protein–ligand interactions

are analyzed. The aim of the pK_a calculation is to study the shift of the pK_a values of ligands upon protein binding.

For calculating the pK_a shifts, all residues within a radius of 12 Å around the guanine binding pocket were selected (Table 3). The protonation states of the considered amino acids are responsible for changes of the pK_a values of the ligands upon binding to the protein.

A first calculation of the unoccupied binding pocket at different pH values is necessary to study the protonation states of the participating residues (Table 3). The calculation only considers side chains where the protonation state might change under the applied pH conditions (so-called titratable groups).

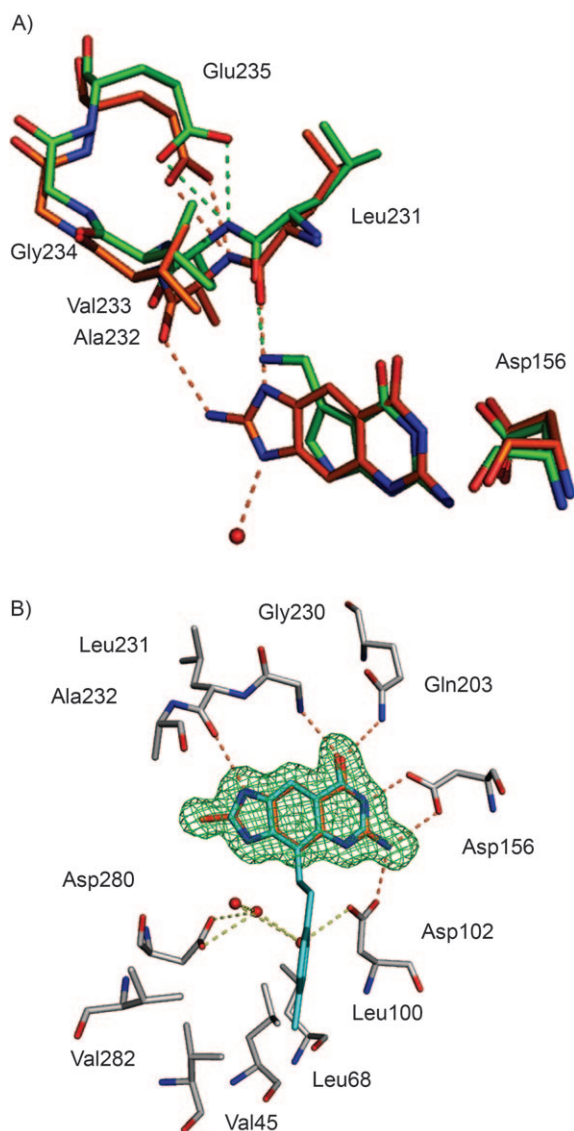


Figure 2. A) Superposition of the TGT complexes with preQ₁ (PDB ID: 1P0E; carbon = green, nitrogen = blue, oxygen = red) and compound **5** (PDB ID: 2Z7K, carbon = orange, nitrogen = blue, oxygen = red). The shift in the backbone of the protein between the residues 230 and 235 is about 1 Å. The carbonyl group of Leu231 is orientated into the guanine binding pocket and a hydrogen bond between preQ₁ or **5** is formed (for **5**, additional hydrogen bonds to Ala232 and a close by water molecule W (red), which is part of the water cluster solvating the two catalytic aspartate side chains, are possible). The conformation of Leu231 is stabilized by the deprotonated Glu235. Hydrogen bonds in complex with preQ₁ are shown as dashed lines in green and for the complex with **5** in orange. B) TGT in complex with **4** (PDB ID: 3C2Y, carbon = gray, nitrogen = blue, oxygen = red). In the guanine binding pocket the 2-methyl-*lin*-benzoguanine skeleton of **4** (orange) fits perfectly into the difference electron density (green). **4** is fixed in the binding pocket by several hydrogen bonds to the surrounding amino acids (orange dashes). Three water molecules are bound between the catalytically active aspartates (red; hydrogen pattern = yellow dashes). Superimposed is a ligand (PDB ID: 1Y5W; carbon = cyan, nitrogen = blue, oxygen = red) with a hydrophobic side chain addressing a small hydrophobic subpocket that is created by Val282, Val45, Leu68, and Leu100. The hydrophobic side chain disturbs the water molecules between Asp102 and Asp280 upon binding.

The study was performed at three different pH conditions (5.5, 7.0, and 8.5). The results are listed in Table 3. A value of 1.00

corresponds to 100% and a value of 0 to 0% protonation or deprotonation of a titratable group. The deprotonation of Asp102 and Asp280, as previously assumed for the catalytic reaction, was verified by the calculation for all three pH conditions.^[7] The deprotonation of Asp280 allows the nucleophilic attack towards the ribose 34 C1' atom during the base-exchange reaction.

Recently, the importance of Glu235 as a trigger residue for the peptide flip of Leu231 was suggested.^[14] Depending on the substrate bound in the guanine binding pocket, either the NH group or the CO group of Leu231 is facing the carboxyl functionality of Glu235 (Figure 2A). Based on a pK_a value of 2.7 in the calculation, Glu235 would be considered as charged at all pH conditions while NH is facing Glu235 (Table 3).

As mentioned, the pK_a values for the ligands were experimentally determined in aqueous solution.^[15] A shift of approximately one logarithmic unit has been measured for the imidazolium or 2-aminoimidazolium moiety comparing the *lin*-benzoguanines (5.2–5.4) and the 2-amino-*lin*-benzoguanines (5.8–6.3; Table 2).

The pK_a calculation for the complex structures is performed at pH 7. For the inhibitors, the experimentally determined pK_a values are taken as starting values. The calculation reveals, that upon complexation all pK_a values of the ligands are shifted towards basic range, overall by about 1.2 to 2.4 logarithmic units (Table 2). As described above, this shift suggests a permanent protonation of the ligands at the binding site under assay conditions (pH 7.3). The protonation of the guanidinium group creates a positive charge on this molecular portion. It increases the strength of the hydrogen bond between the imidazolium-type nitrogen atom of the ligand and the carbonyl group of Leu231. Towards the inner of the protein, the NH group of the amide bond of Leu231 is stabilized by the deprotonated Glu235. The resulting arrangement suggests formation of a hydrogen bond with charge-assisted salt bridge character. The charged interaction enhances binding affinity of the 2-amino-*lin*-benzoguanines towards TGT.

Crystal structures

For the parent skeleton *lin*-benzoguanine and the modified 2-amino-*lin*-benzoguanines crystal structures in complex with TGT were determined (represented by using **5** in Figure 1B). The binding mode is similar to the one of preQ₁ (Figure 1A). Accordingly, the peptide bond between Leu231 and Ala232 is found in its flipped orientation with the carbonyl group exposed towards the recognition site (Figure 2A). For the newly synthesized compounds **4**, **5**, **7**, and **9**, binary complexes with *Z. mobilis* TGT could be obtained. The maximum resolution achieved by the structure determinations varies from 1.28 Å to 1.78 Å. Details about the refinement statistics are given in Table 4 and information about the data collection can be found in Materials and Methods. The binding mode, previously discovered for **3**, is confirmed by **4**, **5**, **7**, and **9**. As expected, the water network between Asp102 and Asp280 is not disrupted. The peptide bond between Leu231 and Ala232 is flipped

Table 3. Calculation of pK_a values of different titratable groups of TGT active site.

Residue ^[a]	pK _a	pH 5.5			pH 7.0			pH 8.5		
		protonated	:	deprotonated	protonated	:	deprotonated	protonated	:	deprotonated
Cys158	10.7	1.00	:	0	1.00	:	0	0.99	:	0.01
Cys281	8.4	1.00	:	0	0.96	:	0.04	0.46	:	0.54
Asp156	4.1	0.04	:	0.96	0	:	1.00	0	:	1.00
Asp102	−0.4	0	:	1.00	0	:	1.00	0	:	1.00
Asp280	1.7	0	:	1.00	0	:	1.00	0	:	1.00
Lys125	10.3	1.00	:	0	1.00	:	0	0.98	:	0.02
Lys264	12.2	1.00	:	0	1.00	:	0	1.00	:	0
Glu157	4.9	0.18	:	0.82	0.01	:	0.99	0	:	1.00
Glu235	2.7	0	:	1.00	0	:	1.00	0	:	1.00
Tyr072	11.3	1.00	:	0	1.00	:	0	1.00	:	0
Tyr106	11.6	1.00	:	0	1.00	:	0	1.00	:	0
Tyr161	9.7	1.00	:	0	1.00	:	0	0.94	:	0.06
Tyr258	14.4	1.00	:	0	1.00	:	0	1.00	:	0

[a] For the calculation of the pK_a values all titratable groups within a radius of 12 Å around the active site were determined (C γ of Tyr106 was taken as origin of the selection). Each residue has an assigned pK_a value based on the modified peoe_{pb} charges. For each residue, the ratio of protonation vs. deprotonation at three different pH values (5.5, 7.0, and 8.5) is determined (a value of 1.00 corresponds to 100% protonation or deprotonation).

and the carbonyl oxygen forms a hydrogen bond to N1 of the ligand scaffold.

For cocrystallization and soaking of TGT crystals two conditions have been discovered, one at pH 5.5 and another at pH 8.5. With respect to structures of TGT in complex with preQ₁ significant geometric differences, depending on pH conditions, have been observed.^[20] At pH 5.5 (PDB ID: 2Z1X), Asp102 is rotated to 75% into the guanine binding pocket whereas at pH 8.5 (PDB ID: 2NQZ) the same residue is oriented to 100% out of the pocket. In order to evaluate whether the presence of a ligand can provoke the inwards orientation of Asp102, **7** was soaked into the apo crystal at a pH of 8.5. The observed electron density of **7** in complex with TGT discloses that Asp102 is actually rotated into the binding pocket. Obviously, a rotation of Asp102 is induced by the presence of the *lin*-benzoguanine scaffold. This is in contrast to previously studied protein–ligand complexes exhibiting different scaffolds. In all these examples, rotation of Asp102 towards the bound ligand was not observed at pH 8.5.

For 2-methyl-*lin*-benzoguanine (**4**), a dataset with a maximum resolution of 1.78 Å could be collected. The above-described 2.7-fold increase in binding affinity compared to the unsubstituted *lin*-benzoguanine (**3**) can be ascribed to an additional efficient van der Waals contact to C β of Ala232 (calculated with the program *contacsym*,^[21] Figure 3).

By the introduction of the alkylamine substituent in 2-position, a dramatic increase of the binding affinity was observed. The analysis of the complexes with **5**, **9**, and **10** stresses an additional hydrogen bond to the carbonyl group of Ala232 exhibiting an average length of 2.8 Å (representatively shown for **5**, Figures 1B and 2A).

Based on the performed in silico pK_a studies, the protonation of **5–10** appears most likely. With the complexes of **5**, **7**, and **10**, this hypothesis has been further validated. A data set of TGT in complex with **5** could be collected to a maximum resolution of 1.28 Å. Based on the high resolution of this structure, a detailed picture of the protein could be obtained, in-

dicating split conformations for several amino acids. The inhibitor in the guanine binding site is well defined and forms hydrogen bonds to Leu231, Ala232, Asp156, and Asp102 (Figure 4). The superposition of 2-amino-*lin*-benzoguanine (**5**) and preQ₁ in complex with TGT reflects a very similar hydrogen bond length towards the carbonyl group of Leu231 (2.7 Å preQ₁, PDB ID: 1P0E; 2.8 Å **5**, PDB ID: 2Z7K) (Figure 2A and B) although the inhibitor has no extracyclic amino function. In order to maintain the same distance, the backbone between residue 231 and 235 has been shifted towards the inhibitor and the hydrogen bond is formed to the nitrogen atom of the imidazole moiety facing the CO group of Leu231.

In **7** (6-amino-2-[(thiophene-2-ylmethyl)-amino]-1,7-dihydroimidazo [4,5g]quinazolin-8-one), a thiophene-2-methylene moiety has been chosen as substituent to grow the inhibition skeleton towards the ribose 33 binding pocket (Figure 5A). Surprisingly, no properly defined electron density could be observed for the sulfur-containing ring system. At most, an ethyl group could be built into the electron density. The poorly defined electron density indicates that the thiophene ring is probably scattered over multiple configurations. By taking the complex of TGT with bound tRNA as a reference for the superposition with the present complex, it is possible to model the thiophene ring into the same region of the binding site as occupied by ribose 33 in the natural substrate (Figure 5A). This superposition suggests that the methylene spacer has the appropriate size to reach out into the ribose 33 binding pocket and to correctly place a terminally decorated thiophene moiety.

Interestingly, the crystal structure shows a split conformation for Asp280 and Cys281 (Figure 5B). This observation is particularly surprising as Asp280 is involved as a nucleophile in the catalytic mechanism. It might be possible that the thiophene ring perturbs to some degree the conformation of Asp280. Subsequently, the steric displacement of the thiophene moiety translates into a 180° rotation of Cys281 from an orientation

Table 4. Data collection and refinement statistics for TGT in complex with **4**, **5**, **7**, and **9**.

Crystal data	4	5	7	9
PDB ID	3C2Y	2Z7K	3C2Z	3C2N
A) Data collection and processing				
no. crystals used	1	1	1	1
λ [Å]	1.5418	0.97803	1.5418	0.97803
space group	C2	C2	C2	C2
unit cell parameters				
a [Å]	90.3	90.5	90.2	90.7
b [Å]	64.8	65.1	64.7	64.5
c [Å]	70.3	70.6	70.4	70.3
β [°]	96.0	96.2	96.0	95.5
B) Diffraction data				
resolution range [Å]	50–1.78	30–1.28	50–1.65	25–1.58
unique reflections	36 907	10 2059	48 527	54 350
	(1780) ^[a]	(5228) ^[a]	(2416) ^[a]	(2524) ^[a]
$R(I)_{\text{sym}}$ [%] ^[b]	5.5 (37.0) ^[a]	3.8 (24.9) ^[a]	6.0 (51.0) ^[a]	4.4 (22.3) ^[a]
completeness [%]	95.0	99.6 (97.4) ^[a]	99.9	98.0
	(92.3) ^[a]		(99.5) ^[a]	(91.1) ^[a]
redundancy	1.9 (1.9) ^[a]	2.7 (2.5) ^[a]	3.7 (3.2) ^[a]	3.0 (2.1) ^[a]
$I/\sigma(I)$	15.0 (2.3) ^[a]	21.4 (3.8) ^[a]	20.6 (2.4) ^[a]	23.0 (4.0) ^[a]
C) Refinement				
program used	SHELXL	SHELXL	SHELXL	SHELXL
for refinement				
resolution range [Å]	10–1.78	10–1.28	10–1.65	10–1.58
reflections used	35 094	96 866	46 663	52 369
in refinement				
final R values				
R_{free} (F_o ; $F_o > 4\sigma$) ^[d]	21.4	18.6	21.7	21.7
	(15.0) ^[a]	(14.8) ^[a]	(20.5) ^[a]	(20.6) ^[a]
R_{work} (F_o ; $F_o > 4\sigma$) ^[c]	16.4	16.2	17.2	16.8
	(14.0) ^[a]	(14.0) ^[a]	(16.2) ^[a]	(16.7) ^[a]
no. of atoms (non-hydrogen)				
protein atoms	2809	2895	2760	2714
water molecules	274	375	233	302
ligand atoms	16	15	18	18
RMSD, angle [°]	2.1	2.4	2.3	2.3
RMSD, bond [Å]	0.009	0.015	0.010	0.010
Ramachandran plot ^[e]				
most favored regions	95.5	95.1	95.0	94.6
[%]				
additionally allowed	4.2	4.6	4.3	5.1
regions [%]				
generously allowed	0.3	0.3	0.7	0.3
regions [%]				
mean B -factors [Å ²]				
protein atoms	15.4	13.7	13.5	16.1
water molecules	27.0	29.0	23.6	30.7
ligand atoms	12.1	11.4	15.3	15.3

[a] Values in parenthesis are statistics for the highest-resolution shell. [b] $R(I)_{\text{sym}} = [\sum_i \sum_j |I_i(h) - I_j(h)| / \sum_i \sum_j I_i(h)] \times 100$, where $\langle I(h) \rangle$ is the mean of the $I(h)$ observation of reflection h . [c] $R_{\text{work}} = \sum_{hkl} |F_o - F_c| / \sum_{hkl} |F_o|$. [d] R_{free} was calculated as for R_{work} but on 5% of the data that were excluded from refinement. [e] From Procheck.

towards the surface of the protein into the cavity that is usually occupied by uracil 35 in the natural substrate.

The best binding affinity is observed for 6-amino-2-(2-morpholin-4-yl-ethylamino)-1,7-dihydro-imidazo[4,5g]quinazolin-8-one (**9**). This compound shows an affinity of 6 nM. The skeleton does not fit entirely into the difference electron density. The

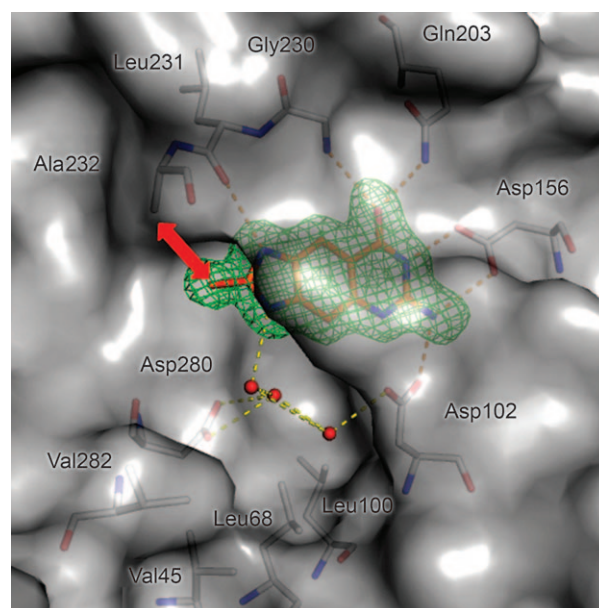


Figure 3. Crystal structure of **4** in the binding pocket of TGT determined at 1.78 Å resolution. The solvent-accessible surface of the protein is shown in gray. In addition some selected amino acids (carbon = gray, nitrogen = blue, oxygen = red) in the guanine binding pocket recognizing **4** are shown. The hydrogen bonds between TGT and **4** are highlighted by yellow dashed lines. Compound **4** is contoured at 2.5σ in the $|F_o| - |F_c|$ density map (green) of the structural model refined without the ligand. The ligand (carbon = orange, nitrogen = blue, oxygen = red) is well depicted in the binding pocket. Several hydrogen bonds (orange dashes) are formed between the ligand and the protein. A short van der Waals interaction (3.3 Å, red arrow) between the methyl group in 2-position of the *lin*-benzoguanine scaffold and C_β of Ala232 is present. In addition, three water molecules (red) are bound between Asp102 and Asp280 (H-bonds: yellow dashes).

ethyl linker between the 2-amino-*lin*-benzoguanine and the morpholino moiety can be assigned to difference electron density ($|F_o| - |F_c|$ map at 2.5σ) but for the highly scattered morpholino ring, no properly defined electron density could be observed (Figure 6A).

In a previous communication, the structure of a derivative with a naphthyl side chain added to 2-amino-*lin*-benzoguanine (**8**) skeleton has been presented.^[15] In this complex, it was partly possible to assign the side chain of the ligand to the difference electron density (PDB ID: 2QZR). Interestingly, the lower part of the naphthyl moiety, which is covalently attached to the *lin*-benzoguanine skeleton is visible in the difference electron density. The upper six-membered ring is ill-defined. Likely this corresponds to a kind of wiggling motion of the naphthyl moiety perpendicular to the protein surface.

Compared to the complex of **9**, the hydrogen bonds between the guanidinium moiety of **8** and the carbonyl oxygen atom of Leu231 and Ala232 are expanded (hydrogen bond to Leu231: **5**: 2.8 Å; **8**: 3.0 Å; to Ala232: **9**: 2.7 Å; **8**: 3.6 Å; Figure 7). Obviously, the naphthyl side chain of **8** pushes the *lin*-benzoguanine scaffold away from Ala232. Accordingly, it induces a slight rotation of Tyr106 and Val233. Tyr106 closes up the binding pocket once no ligand or substrate is accommodated by TGT. In the apo structure, it forms a hydrogen bond to Asp156. When a ligand is entering the guanine binding

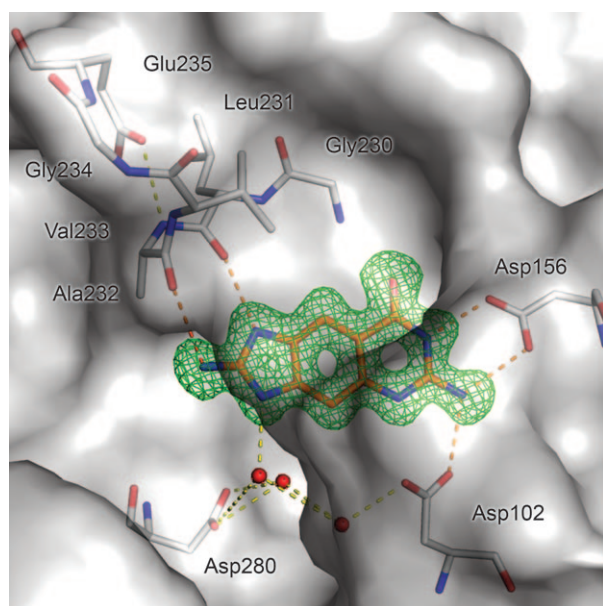


Figure 4. Surface presentation (gray) of TGT in complex with **5** determined at 1.28 Å. In the guanine binding pocket **5** is shown in orange (carbon = orange, nitrogen = blue, oxygen = red) and the surrounding amino acids are shown in gray (carbon = gray, nitrogen = blue, oxygen = red). The $|F_o| - |F_c|$ density map of **5** of the structural model refined without the ligand is shown at 2.5σ (green). The inhibitor occupies completely the deep binding pocket of guanine. Several hydrogen bonds (orange dashes) are formed between **5** and the protein. Three water molecules are placed between the carboxyl groups of Asp102 and Asp280 (red, hydrogen bonds = yellow dashes).

pocket, Tyr106 performs a π -stacking with the aromatic ring system of the bound ligand. In the case of binding the naphthyl derivative, the position of Tyr106 is distorted. In addition,

Val233 is rotated out of the binding pocket. The distance between Tyr106 C $_{\epsilon}$ and Val233 C $_{\beta}$ increases in the complex of **8** (6.7 Å) compared to the complex of **9** (5.4 Å) leading to an opening of the guanine binding pocket (Figure 7). Astonishingly, the complex of **8** is up to now the only example where the side chain of the inhibitor could be fitted to a reasonably defined electron density. Probably, the binding mode with an ordered side chain orientation is based on a steric interaction of the naphthyl moiety with Tyr106, leading to a shifted placement of the *lin*-benzoguanine scaffold in the guanine recognition pocket. Nevertheless, the affinity falls into the same range as for other ligands exhibiting a guanidinium-type moiety. Therefore, the opening of the guanine binding pocket has supposedly no impact on the affinity of ligand binding.

All *lin*-benzoguanines are based on a tricyclic aromatic scaffold. It is remarkable that this ring system is not always planar (Figure 8). In complex with **5**, **7**, and **9**, the electron density for the scaffold is bent out of plane by approximately 7.5°. In a refinement cycle, where the ligand was artificially constrained to a planar geometry, residual negative and positive difference electron density has been received. The unexpected non-planarity can likely be explained by a protonation of the conjugated system of the guanidinium-like moiety, providing further crystallographic evidence that the 2-amino-*lin*-benzoguanines are protonated upon binding to TGT.

Docking experiments

For the complexes of **7** and **9** with TGT, it was not possible to fit the side chain of the inhibitor into the electron density. Only some weak peaks of residual electron density are visible (Figures 5A and 6A). In order to estimate possible orientations

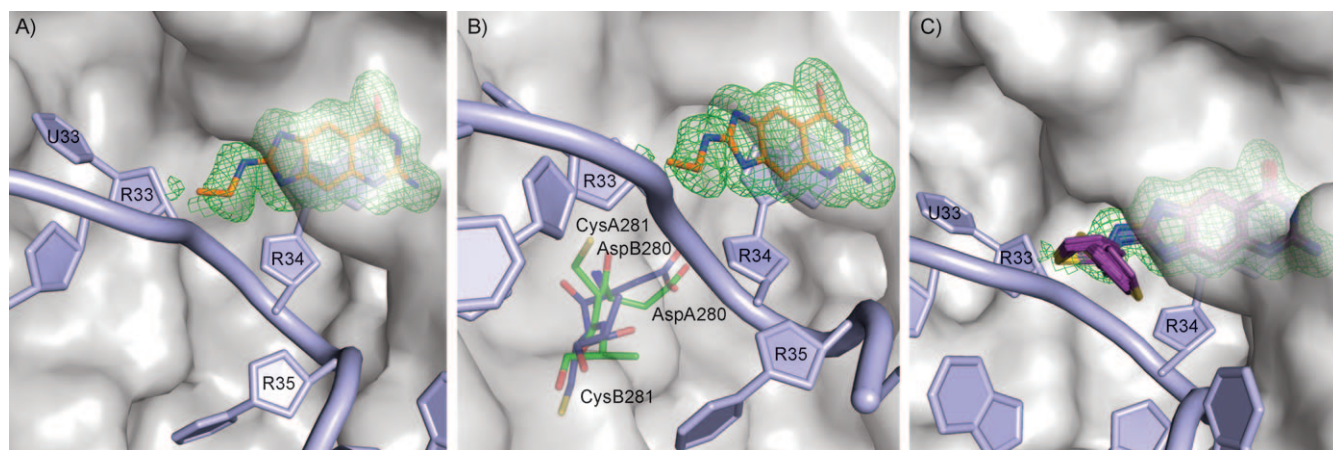


Figure 5. Superimposition of TGT in complex with a preQ₁ modified tRNA loop (PDB ID: 1Q2S; blue, only the ligand is shown) and compound **7** (PDB ID: 3C2Z; protein: surface presentation in gray; ligand: carbon = orange, nitrogen = blue, oxygen = red). For the 2-amino-*lin*-benzoguanine scaffold the difference electron density is well defined ($|F_o| - |F_c|$ density map at 2.5σ in green for the structural model refined without the ligand). A) The thiophene ring of **7** is dislocated, but based on the position of the ethyl linker a localization of the thiophene ring similar to ribose 33 can be anticipated. B) For Asp280 and Cys281 two conformations are refined (conformation A: carbon = green, nitrogen = blue, oxygen = red, sulfur = yellow; conformation B) carbon = blue, nitrogen = blue, oxygen = red, sulfur = yellow). Conformation A orients the thiol group of Cys281 towards the surface of the protein whereas in conformation B the thiol group is rotated by 180° and faces to the interior of the protein. In addition, the position of Asp280 is slightly shifted; this is especially remarkable because Asp performs the nucleophilic attack towards C1' of the ribose during the base-exchange reaction. C) Superposition of 20 docking solutions (carbon = purple, nitrogen = blue, oxygen = red; sulfur = yellow) generated with the program GOLD. The sulfur atom of the thiophene ring is fitted into the difference electron density, as it would contribute most as the strongest scatter to the density.

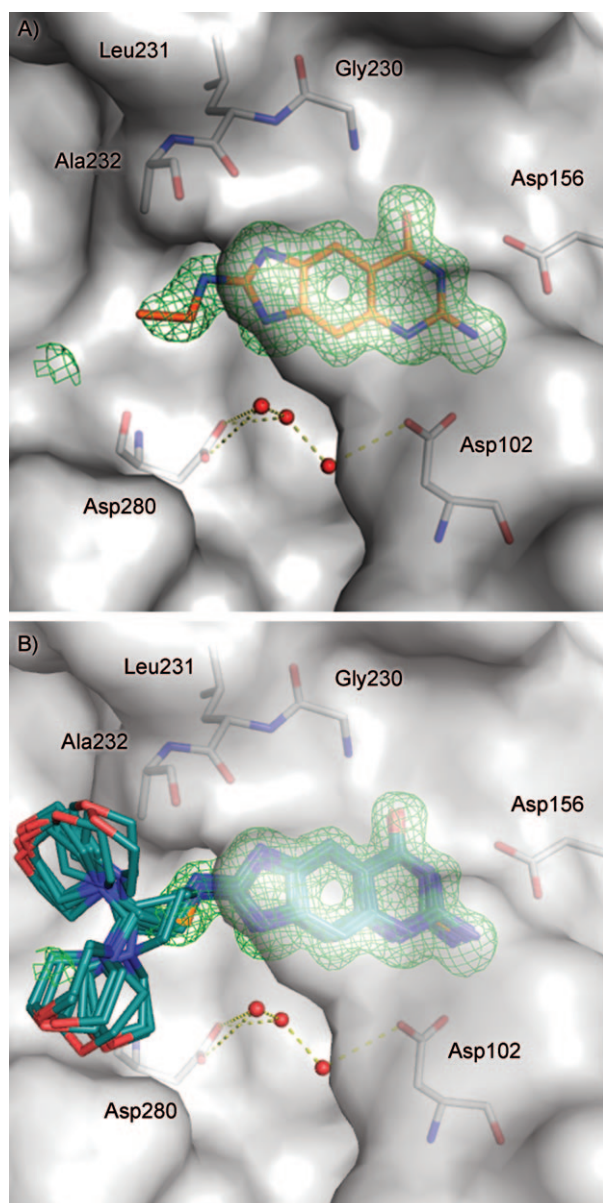


Figure 6. Surface representation of TGT in gray; ligand: carbon = orange, nitrogen = blue, oxygen = red; $|F_o| - |F_c|$ density map at 2.5σ in green of the structural model refined without the ligand **9** in the guanine binding pocket. The morpholino ring system of **9** is not shown because no properly defined electron density could be observed during refinement. B) A total of 20 docking solutions derived with the program GOLD are superimposed on the complex with **9**. The docking solutions show that the morpholino side chain is solvent exposed and multiple conformations are possible.

of the side chain, docking experiments by using the program GOLD were performed.^[22] In Figure 5C, the docking solutions for **7** are visualized. The docked geometries show a cluster for the side chain orientations close to the ribose 33 binding site as already indicated by the crystal structure. For **9**, the docking delivers two clusters (Figure 6B) for the morpholino side chain. The placement of the docking solutions supports the assumption that the side chain is rather solvent exposed, and no par-

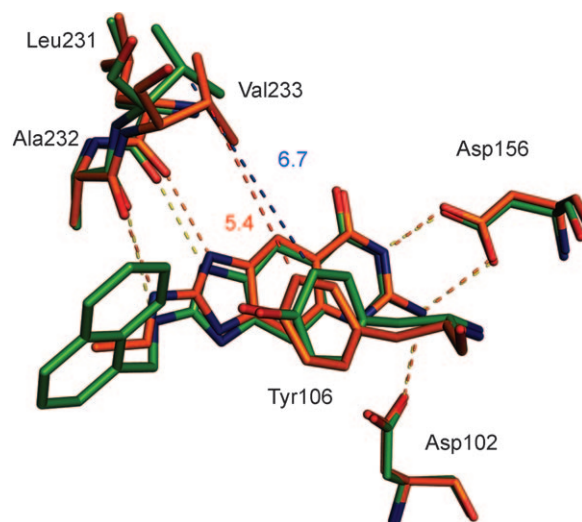


Figure 7. Superposition of TGT in complex with **8** (PDB ID: 2QZR; carbon = green, nitrogen = blue, oxygen = red, hydrogen bonds = orange dashes) and **9** (PDB ID: 3C2N; carbon = orange, nitrogen = blue, oxygen = red, hydrogen bonds = yellow dashes). The side chain of Val233 is shifted in the complex of **8**, which results in a larger distance between Tyr106 and Val233 (**8**: 6.7 Å, blue dashes; **9**: 5.4 Å, red dashes).

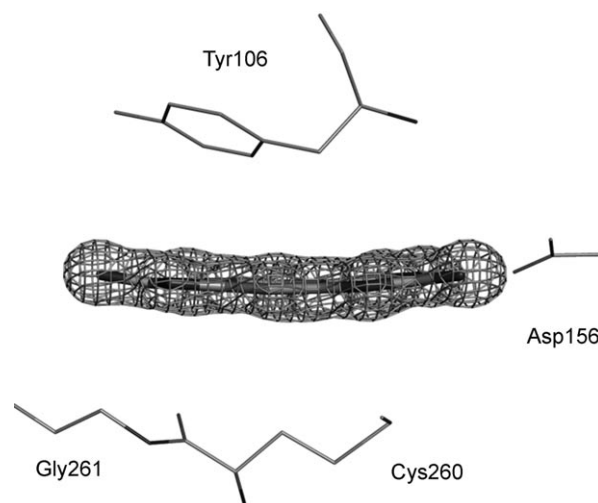


Figure 8. Complex of **5** and TGT. The $|F_o| - |F_c|$ density map of **5** of the structural model refined without the ligand is shown at 2.5σ in green. The inhibitor is slightly bent in the guanine binding pocket (approximately 7.5°).

ticular arrangement with a set of preferred interactions appears possible.

Conclusions

The synthesis of new TGT inhibitors with the aim to address the ribose 33 binding pocket led to a dramatic increase in binding affinity. The modification of the scaffold *lin*-benzoguanine to synthetically easily accessible 2-amino-*lin*-benzoguanines changed the characteristics of our inhibitors. With this skeleton, it is now possible to form an additional hydrogen bond at the far end of the guanine binding pocket between the carbonyl group of Ala232 and the exocyclic amino function

of the inhibitor (Figure 4). However, the most important contribution to the increased binding affinity results from a change of the physico-chemical properties of the scaffold. With the introduction of the guanidinium functionality, a permanent charge is most likely created on this portion of the inhibitor which results in the formation of a charge-assisted hydrogen bond to the carbonyl group of Leu231. This interaction is further stabilized by the negative charge of the deprotonated Glu235 facing the NH of Leu231 from the back. For the evaluation of the charge-assisted hydrogen bond between the ligands and TGT, we performed a novel application of *in silico* pK_a calculation. So far the pK_a calculation with modified peoe_{pb} charges were only used to characterize the protonation state in active sites of HIV protease and other proteases, such as trypsin and thrombin, but it was never consulted to explain trends in affinities.^[23,24] This evaluation shows that pK_a calculations can also be applied to study affinity relationships of protein–ligand complexes. The results of the pK_a calculation support the increasing basic character of our inhibitors, particularly once bound to the protein, which strengthens the interaction to Leu231.

The crystal structures emphasize the conserved binding mode of the scaffold of the *lin*-benzoguanines in the guanine binding pocket. The introduced side chains in 2-position can bind to the ribose 33 binding pocket. The disruption of the water cluster network which had a detrimental effect on the binding energy in previous studies could not be observed for **4–10**. With our new design strategy we could bear the first nanomolar TGT inhibitors.

An additional interesting feature can be observed from the complexes of **7** and **9**, where it is not possible to fit the complete side chain of the ligand into the electron density. Nevertheless, the binding affinity is still increased compared to the complex of **6** (for **7** the increase is 1.7-fold, for **9** it is nearly tenfold). The side chain is not fixed in one preferred orientation and in our docking experiments the thiophene and the morpholino moiety are scattered over multiple conformations. The residual mobility of the side chain in the protein-bound state obviously enhances binding affinity of a less intimate and shape-complementary complex between ligand and protein. Certainly, upon complex formation, the overall residual conformational entropy is reduced, but is usually compensated for by an enhanced enthalpy contribution experienced by the newly formed interactions with the ligand. In the present case, the residual amount of degrees of freedom resulting from the still activated conformational mobility of the side chain is beneficial for the entropic contribution to binding. A partial loss of degrees of freedom pays a smaller price in entropy. Overall, an enhanced Gibbs free energy of binding is observed, particularly for **9**. As important message from this study, it can be concluded that enhancement of binding affinity does not necessarily correlate with one unique and well-defined shape-complementary conformation of the ligand or its portions. Recently, we could report a similar case where the complete disorder of a ligand side chain was not detrimental to binding affinity.^[25] In this case, the binding constant, a typical free energy entity, is determined predominantly by either an enthalpic and en-

tropic contribution. Possibly, our traditional thinking in terms of lead optimization in medical chemistry is too strongly biased towards an enthalpic view, only accepting structural evidence once a properly defined ligand configuration can be discovered in the difference electron density of the complex. Also, a beneficial residual configuration entropy contribution can result in an improved protein–ligand binding.

Experimental Section

Trapping experiment: For the characterization of the kinetic properties of the ligand 5 μM *Z. mobilis* TGT, 100 μM *E. coli* tRNA^{Tyr}, and 10 mM of the particular inhibitor dissolved in DMSO were incubated for 1 h at 25 °C. Furthermore, SDS loading buffer (10 μL) was added, and the mixture was incubated for an additional hour at 25 °C. Each sample (5 μL) was loaded onto a 15% SDS gel and stained with 0.1% Coomassie brilliant blue.^[13] For a competitive inhibitor only one band was visible on the SDS gel representing TGT. In contrast two bands were obtained on the SDS gel for a mixed inhibition, one for TGT and an additional one for TGT in complex with tRNA.

Inhibition constant determination: The inhibitor kinetic constants were acquired in an assay solution of 19 nM *Z. mobilis* TGT, 200 mM HEPES buffer, pH 7.3, 20 mM MgCl₂, 2.95 μM Tween 20 containing both substrates, 8-[³H]-guanine HCl and *E. coli* tRNA^{Tyr} in various concentrations. In addition, the assay solution contained 5% DMSO to ensure solubility of the inhibitors.

The assay reaction was started by adding the substrates and its turnover was measured by taking an aliquot (15 μL) four times, at three minute intervals. The aliquots were directly transferred to glass fiber filters (GC-F, Whatman), quenched in 10% (w/v) trichloroacetic acid (20 min), and washed in 5% (w/v) trichloroacetic acid (2 \times 7 min) to wash out tRNA-unbound 8-[³H]-guanine. The filters were dried at 60 °C, and tRNA-incorporated tritium was quantified by using liquid scintillation counting.

For the calculation of the inhibitor constants, the method introduced by Grädler et al. and modified by Meyer et al. was applied.^[6,13] Here, TGT was incubated with 20 μM 8-[³H]-guanine, 1.5 μM tRNA^{Tyr} in the presence of five different inhibitor concentrations. The initial velocity of the base-exchange reaction was decreased by the added inhibitor. This enabled the calculation of competitive inhibition constants for each inhibitor.

In silico pK_a calculations: A consistent charge model was produced by a modified version of the charge distribution algorithm that was suggested by Gasteiger and Marsili, named “partial equalization of orbital electronegativities” (PEOE).^[26]

The *in silico* calculation was based on the charge distribution in the active site of TGT derived from the modified peoe_{pb} charges. Another value important for the calculation was the assigned dielectric constant ϵ . For the binding site an approximate estimation of this value was crucial. To adjust a reasonable value that closely resembled the properties of the binding site, we tested two different values: $\epsilon = 10$ and $\epsilon = 20$. A shift of about one logarithmic unit to a more basic range for all inhibitor complexes was obtained by using a dielectric constant of $\epsilon = 20$. At a value of $\epsilon = 10$, the pK_a shift was larger (2.4–4.4) and resulted in values that appeared exaggerated to correctly represent the observed effects of the formed protein–ligand complex.

For the calculation of the pK_a values all titratable groups in a radius of 12 Å around the active site were determined (C γ of Tyr106 was taken as centre of the selection; Table 3). With the program REDUCE all hydrogens were added to the protein where all acidic amino acids were deprotonated and basic amino acids were protonated.^[27]

SYBYL ligand atom types were assigned to the ligands to generate its unprotonated and its protonated form. Based on the modified peoe_pb charges a total net charge was assigned for both ligand states. After this preparation, the Poisson–Boltzmann calculation was started. The resulting pK_a shifts were listed in Table 2 at a pH of 7.0.

Z. mobilis TGT crystallization: *Z. mobilis* TGT was cloned and expressed in *E. coli*. This procedure and the purification of the protein have been described in detail elsewhere.^[1,28,29] Crystals appropriate for soaking ligands were obtained in a two-step procedure. First microcrystals were grown via hanging-drop, vapor diffusion method at 273 K. Therefore, protein solution (2 μ L; 16.8 mg mL⁻¹ TGT, 2 M NaCl, 10 mM TRIS-HCl pH 7.8, 1 mM EDTA, 1 mM DTT) was mixed with reservoir solution (2 μ L) at pH 8.5 (8% (w/v) PEG 8000, 100 mM TRIS-HCl, 1 mM DTT, 10% DMSO) or at pH 5.5 (13% (w/v) PEG 8000, 100 mM MES, 1 mM DTT, 10% DMSO) to a droplet. During a few days microcrystals with the size of 0.05 mm³ were observed. In a second step, a macro-seeding was performed where the crystals grew to a size of about 0.7 × 0.7 × 0.2 mm. For the macro-seeding one micro-crystal was transferred to a droplet with protein solution (2 μ L) and reservoir solution (2 μ L). The reservoir solution was similar to the one used in the first step but had a decreased concentration of PEG 8000 (pH 8.5: 5% (w/v); pH 5.5: 8% (w/v)). The ligands were dissolved in DMSO and mixed with reservoir solution to a final concentration of 5 mM. A single crystal was introduced into a droplet of this mixture and soaked for about one day.

Data collection: The soaked crystals were transferred for about 10 s into a solution containing glycerol as cryo-protectant (pH 8.5: 50 mM Tris-HCl, 0.5 mM DTT, 0.3 M NaCl, 2% DMSO, 4% PEG 8000, 30% glycerol; pH 5.5: 50 mM MES, 0.5 mM DTT, 0.3 M NaCl, 2% DMSO, 4% PEG 8000, 30% glycerol) and afterwards directly flash-frozen in liquid N₂.

Data sets for **4** and **7** were collected at cryo conditions (100 K) with Cu α radiation (λ = 1.5418 Å) by using a Rigaku RU-H300R rotating-anode generator at 50 kV and 90 mA equipped with focusing mirrors (Xenocs mirrors) and an R-Axis IV or R-Axis IV++ (MSC, USA) image-plate system.

The data sets for **5** and **9** were collected at cryo conditions (100 K) as well at the BESSY-PSF Beamline 14.2 in Berlin. Synchrotron radiation (at wavelength λ = 0.97803 Å) was used. A MAR CCD 165 mm detector was utilized for data collection.

The protein crystallizes in the monoclinic space group C2 containing one monomer per asymmetric unit with Matthews coefficients of 2.3–2.4. Unit cell dimensions for all crystals are listed in Table 3. Data processing and scaling were performed by using the HKL2000 package. Data collection and processing statistics are given (Table 3).^[30]

Structure determination and refinement: For the complexes of **4**, **5**, **7**, and **9** the coordinates of the TGT apo structure (1P0D) were directly used for an initial rigid-body refinement and a cycle of maximum likelihood energy minimization, simulated annealing, and B-factor refinement by using the CNS program package was performed.^[31]

The high resolution of the structures allows a further refinement with the program SHELXL.^[32] Here, at least 20 cycles of conjugate gradient minimization were performed with default restraints on bonding geometry and B-values: 5% of all data were used for R_{free} calculation. Amino acid side chains were fit to σ_A -weighted $|F_o| - |F_c|$ and $2|F_o| - |F_c|$ electron density maps by using COOT.^[33] In the electron density water, glycerol molecules, and the ligand were located, and subsequently included to further refinement cycles. In a final refinement, riding H-atoms were placed for the protein (not for ligand) without using additional parameters. All final validation of the model was performed with PROCHECK.^[34]

Figure were prepared by using Isis Draw and Pymol.^[35]

Protein Data Bank accession codes: The PDB accession code for the TGT in complex with **4** is 3C2Y, **5** is 2Z7K, **7** is 3C2Z, and **9** is 3C2N (also given in Table 3).

Docking experiments: The docking was performed with GOLD 4.0 by using default settings for the genetic algorithm. Inhibitors **7** and **9** were docked 20 times into the guanine binding side of the corresponding crystal structure. The water molecules between the catalytic aspartates were included in the docking run and were kept as fixed.

Acknowledgements

We would like to thank Dr. B. Stengl (University of Marburg, Germany) for his help establishing the practical protocols for the kinetic assay and crystal growth and Dr. P. Czodrowski (University of Marburg, Germany) for his assistance in setting-up the in silico pK_a calculations. We acknowledge the support of the beamline staff at the Protein Structure Factory, BESSY II, Berlin, Germany. The kind support of BMBF (Förderungszeichen 05 ES3XBA/5) covering the travel costs are acknowledged. Work at ETH was supported by the ETH Research Council. We thank Dr. M. Kansy and B. Wagner (Roche, Basel) for the experimental pK_a values.

Keywords: antibiotics • enzymes • molecular modeling • structure–activity relationships • transglycosylases

- [1] C. Romier, K. Reuter, D. Suck, R. Ficner, *EMBO J.* **1996**, *15*, 2850–2857.
- [2] K. Kotloff, J. Winickoff, B. Ivanoff, J. Clemens, D. Swerdlow, P. Sansonetti, G. Adak, M. Levine, *WHO Bull.* **1999**, *77*, 651–666.
- [3] S. Ashkenazi, I. Levy, V. Kazarovskii, Z. Samra, *J. Antimicrob. Chemother.* **2003**, *51*, 427–429.
- [4] J. M. Durand, N. Okada, T. Tobe, M. Watarai, I. Fukuda, T. Suzuki, N. Nakata, K. Komatsu, M. Yoshikawa, C. Sasakawa, *J. Bacteriol.* **1994**, *176*, 4627–4634.
- [5] J. M. Durand, B. Dagberg, B. E. Uhlin, G. R. Björk, *Mol. Microbiol.* **2000**, *35*, 924–935.
- [6] U. Grädler, H. D. Gerber, D. M. Goodenough-Lashua, G. A. Garcia, R. Ficner, K. Reuter, M. T. Stubbs, G. Klebe, *J. Mol. Biol.* **2001**, *306*, 455–467.
- [7] B. Stengl, K. Reuter, G. Klebe, *ChemBioChem* **2005**, *6*, 1926–1939.
- [8] N. Okada, S. Nishimura, *J. Biol. Chem.* **1979**, *254*, 3061–3066.
- [9] S. Nakanishi, T. Ueda, H. Hori, N. Yamazaki, N. Okada, K. Watanabe, *J. Biol. Chem.* **1994**, *269*, 32221–32225.
- [10] A. W. Curnow, G. A. Garcia, *J. Biol. Chem.* **1995**, *270*, 17264–17267.
- [11] W. Xie, X. Liu, R. H. Huang, *Nat. Struct. Mol. Biol.* **2003**, *10*, 781–788.
- [12] D. M. Goodenough-Lashua, G. A. Garcia, *Bioorg. Chem.* **2003**, *31*, 331–344.
- [13] E. A. Meyer, N. Donati, M. Guillot, W. B. Schweizer, F. Diederich, B. Stengl, R. Brenk, K. Reuter, G. Klebe, *Helv. Chim. Acta* **2006**, *89*, 573–597.

- [14] B. Stengl, E. A. Meyer, A. Heine, R. Brenk, F. Diederich, G. Klebe, *J. Mol. Biol.* **2007**, *370*, 492–511.
- [15] S. R. Hörtnner, T. Ritschel, B. Stengl, C. Kramer, W. B. Schweizer, B. Wagner, M. Kansy, G. Klebe, F. Diederich, *Angew. Chem.* **2007**, *119*, 8414–8417; *Angew. Chem. Int. Ed.* **2007**, *46*, 8266–8269.
- [16] B. Stengel, *PhD Thesis*, Philipps University, Marburg (Germany), **2006**.
- [17] W. Xie, X. Liu, R. H. Huang, *Nat. Struct. Biol.* **2003**, *10*, 781–788.
- [18] A. L. Hopkins, C. R. Groom, A. Alex, *Drug. Discov. Today* **2004**, *9*, 430–431.
- [19] P. Czodrowski, I. Dramburg, C. A. Sotriffer, G. Klebe, *Proteins Struct. Funct. Bioinf.* **2006**, *65*, 424–437.
- [20] N. Tidten, B. Stengl, A. Heine, G. A. Garcia, G. Klebe, K. Reuter, *J. Mol. Biol.* **2007**, *374*, 764–776.
- [21] S. Sheriff, W. A. Hendrickson, J. L. Smith, *J. Mol. Biol.* **1987**, *197*, 273–296.
- [22] G. Jones, P. Willett, R. C. Glen, A. R. Leach, R. Taylor, *J. Mol. Biol.* **1997**, *267*, 727–748.
- [23] P. Czodrowski, C. A. Sotriffer, G. Klebe, *J. Chem. Inf. Model.* **2007**, *47*, 1590–1598.
- [24] P. Czodrowski, C. A. Sotriffer, G. Klebe, *J. Mol. Biol.* **2007**, *367*, 1347–1356.
- [25] C. Gerlach, M. Smolinski, H. Steuber, C. A. Sotriffer, A. Heine, D. G. Hangauer, G. Klebe, *Angew. Chem.* **2007**, *119*, 8664–8667; *Angew. Chem. Int. Ed.* **2007**, *46*, 8511–8514.
- [26] J. Gasteiger, M. Marsili, *Tetrahedron* **1980**, *36*, 3219–3228.
- [27] J. M. Word, S. C. Lovell, J. S. Richardson, D. C. Richardson, *J. Mol. Biol.* **1999**, *285*, 1735–1747.
- [28] K. Reuter, R. Ficner, *J. Bacteriol.* **1995**, *177*, 5284–5288.
- [29] C. Romier, R. Ficner, K. Reuter, D. Suck, *Proteins Struct. Funct. Bioinf.* **1996**, *24*, 516–519.
- [30] Z. Otwinowski, W. Minor, *Methods Enzymol.* **1997**, *276*, 307–326.
- [31] A. T. Brünger, P. D. Adams, G. M. Clore, W. L. DeLano, P. Gros, R. W. Grosse-Kunstleve, J.-S. Jiang, J. Kuszewski, M. Nilges, N. S. Pannu, R. J. Read, L. M. Rice, T. Simonson, G. L. Warren, *Acta Crystallogr. Sect. D* **1998**, *54*, 905–921.
- [32] G. M. Sheldrick, T. R. Schneider, *Methods Enzymol.* **1997**, *277*, 319–343.
- [33] P. Emsley, K. Cowtan, *Acta Crystallogr. Sect. D* **2004**, *60*, 2126–2132.
- [34] R. A. Laskowski, M. W. MacArthur, D. S. Moss, J. M. Thornton, *J. Appl. Crystallogr.* **1993**, *26*, 283–291.
- [35] W. L. DeLano, The PyMOL Molecular Graphics System.
- [36] CCG, C.C.G.I., MOE (Molecular Operating Environment), **2005**.
- [37] A. M. Clark, P. Labute, M. Santavy, *J. Chem. Inf. Model.* **2006**, *46*, 1107–1123.

Received: November 27, 2008

Published online on February 6, 2009